An atomistic simulation of the liquid–crystalline phases of sexithiophene

A. Pizzirusso, M. Savini, L. Muccioli* and C. Zannoni

Dipartimento di Chimica Fisica e Inorganica, and INSTM,

Università di Bologna,

Viale Risorgimento 4, 40136 Bologna, Italy

April 26, 2010

Abstract

We have investigated, using atomistic molecular dynamics simulations, the high temperature molecular organization of the linear oligothiophene α-sexithienyl (T6), well known for its organic electronics applications. We have found a smectic and a nematic liquid crystalline phase in the same temperature range where they had been experimentally reported but not fully characterized. We have microscopically characterized the phases and connected the change of mesophase and of order to changes in the T6 conformation and effective shape. T6 phases obtained by rapid cooling from the ordered melts have also been simulated.

1   Introduction

Oligothiophenes represent a class of materials of considerable interest for organic electronics [1] as semiconductors of high mobility [2,3] in organic thin film transistors and organic photovoltaic cells [4]. In this context an important role as p-type materials is played by their conjugated nature that can confer good charge (hole) mobility between molecular units when they are packed in an appropriate morphology. An ideal

---

*corresponding author: email Luca.Muccioli@unibo.it, tel +39 0516446992, fax +39-051-2093690

1

represented by a defect-less crystal with aromatic units closely packed [5], while the reality consists, even in cases where such a crystalline phase exists, of a reduced mobility due to grain boundaries [6,7]. It is thus of interest to consider the possibility of liquid crystalline phases formed by oligothiophenes, since these could be expected to ensure good parallelism between the molecules with the advantage of annealing out defects due to their fluidity [8,9].

In order to explore the possibility of oligothiophene liquid crystal (LC) morphologies, α-sexithiophene (or α-sexithienyl, T6, figure 1) is particularly interesting for a theoretical study. In fact, on one hand its relatively simple structure without alkyl chains makes it relatively easy to model. On the other, a few experimental studies [10,11] indicate that T6 forms at least a LC phase at high temperature, above 585 K, even if the nematic or smectic nature of this mesophase has been questioned. The material itself, beyond being a prototype for more complex substituted oligothiophenes, is not only of academic interest. Indeed good mobilities for an organic semiconductor in the range ~ 0.15 cm^2/Vs in single crystal [12] and $0.01 - 0.03$ cm^2/Vs in thin film and high current on/off ratios ($\sim 10^4$) have been reported [3,13–15]. T6 mobility has also been widely studied in thin films [16] and T6 films have been examined with several techniques such as IR [17], AFM [18], XRD [19] to determine their molecular organization. Other investigations have dealt with the possibility of aligning T6 in a nematic host investigating its polarized photoluminescence [20] or its structure in solution using NMR [21].

The crystalline phases of T6 have also been characterized and different polymorphs have been found according to preparation conditions. In particular a "low temperature" (LT) process with a prolongued sublimation at low pressure and T comprised between 493 K and 513 K produces a monoclinic ($P2_1/n$) structure with $Z = 4$, i. e. 4 molecules per unit cell [22], while a "high temperature" (HT) controlled melt growth (T between 553 K and 588 K) leads to a $P2_1/a$ structure with $Z = 2$ [23]. Both structures are available from the Cambridge Crystallographic Data Centre [24]. Much less attention has been paid to the mesogenic behaviour of sexithiophene. In fact, after a pioneering study by Taliani et al. [10], where it was reported that LT T6 forms a nematic liquid crystal phase when heated above 585 K, and the clearing point was not observed for temperatures up to 623 K, only Destri et al. [11] observed the formation of a mesophase from HT T6 crystal heated up to 578 K, but they were

2

knowledge the high temperature liquid crystal phase of the sexithiophene was not experimentally investigated any further, even if recently similar all-aromatic compounds have attracted some interest for their mesogenic [25, 26] and semiconducting behaviour [27].

Since a lot of effort has been devoted to bulk crystals and thin films, it is surprising that the nature of the liquid crystal phases of T6 and their properties have not been investigated, e. g. in view of optimizing the intermolecular alignment. Part of the reason can be connected to the difficulty of performing detailed experimental investigations at temperatures around or above 600 K. However, theoretical studies of the mesophases are also lacking, while it has recently been shown [28–32] that predictive atomistic simulation can reproduce the nematic–isotropic phase transition temperature of low molecular mass LC such as a cynnamates [28] or cyanobiphenyl homologue series [29–31] to within a few degrees and predict a variety of physical properties such as density, orientational order, NMR dipolar couplings to a few percent error.

In this paper we thus wish to provide an atomistic model of T6, taking into account its flexibility through soft thiophene–thiophene torsional potentials, and use it to perform molecular dynamics simulations over a wide set of temperatures to determine its mesophases. We aim at comparing, where possible, simulated and experimental values as well as to predict static and dynamic observables susceptible to be experimentally determined, such as order parameters and diffusion coefficients. We also investigate the changes in the effective molecular shape that take place in correspondence of the different phases.

2 Force field derivation and testing

The accuracy and predictive capability of a simulation study strongly depends on the quality of the description of the molecular geometry and of intermolecular interactions, which in atomistic simulations are introduced through the molecular mechanics force field (FF) expression and parameters employed. The task of modeling liquid crystal molecules [33] is particularly challenging as the different mesophases are generated by a subtle entropy-enthalpy balance which is reflected in a strong dependence of the transition temperatures on small changes in the FF details, e. g. van der Waals parameters [31] and also on the system size as it will be shown in the following.

[54–57]), and following a standard procedure [57] we have complemented them with atomic partial charges and thiophene-thiophene torsional potential obtained with quantum chemistry methods. In particular atomic charges have been derived with the electrostatic potential fitting method [38] from Gaussian03 calculations performed [39] at the equilibrium geometry of T6 optimized at the B3LYP//cc-pVTZ level of theory. The issue of the inter–ring torsional potential and of the attendant equilibrium geometry of oligothienyls has been investigated for a long time [40, 41] also, examining its dependence on the surrounding medium [42]. The two different sexithiophene (T6) X-ray crystal structures mentioned earlier present perfectly flat geometries: this can be easily understood considering the crystalline packing of the structures and its flattening effect on dihedral angles as also seen for polyphenyls and other oligothiophenes [41, 43]. $2, 2'$ dithienyl (T2) has been studied as a solute in condensed LC phases by ^{1}HNMR [21] and a detailed maximum entropy analysis [44] has shown a preference for a torsional angle of 180°. On the other hand quantum chemical calculations on T2 [45–47], subsequently used by Raos and Marcon for crystal cell simulation of T4 and T6 [48], suggest that the minima energy geometry for T2 in vacuum is at a dihedral angle of about 145° (fig. 2), rather than 180°.

However, the barrier profile obtained theoretically was also shown to depend on the level of the Quantum Mechanics (QM) calculations [46, 48]. To keep into account this issue, in our modelling of T6, aimed at determining the geometry, torsional barriers and charge distribution, we performed several optimizations, using the Gaussian03 software [39] with different methods and basis sets. First we obtained optimized structures with the Hartree-Fock and B3LYP density functional approaches using the STO-3G, 3-21G, 6-31G, cc-pVDZ and cc-pVTZ basis sets. In all cases the equilibrium angle was found to be of 180 degrees, differently from dithiophene [46, 48]. We proceeded then to relaxed scans of the central torsional angle $U(\varphi_1)$ of T6 with B3LYP//cc-pVDZ and cc-pVTZ calculations (fig. 2, black empty squares and cyan triangles). These confirmed the flat geometry for T6, in agreement also with B3LYP/6-31G** calculations on T6 and other fluoroarene-oligothiophene semiconductors [49]. The potential energy surface is indeed very shallow around the minima, both for the SS-anti ($\varphi_1 = 180°$) and for the SS-syn conformation ($\varphi_1 \approx 22°$), which is predicted to be less stable of only 0.68 kcal/mol, hence relatively easy to be populated by increasing temperature. The anti-syn barrier is located at about 90 degrees and needs

4

be very weak (approximately 0.1 kcal/mol above the most stable SS-syn geometry). We have evaluated also the energy profile for the terminal thienyl-thienyl torsion φ_3 (fig. 2, black circles), finding it rather similar to the φ_1 curve with the exception of the anti-syn barrier which decreases to 3.2 kcal/mol.

In the simulation, we used the $U(\varphi) = U(\varphi_1)$ potential for describing all the thienyl-thienyl dihedrals, independently from their position along the T6 molecule. To introduce correctly within the force field the ab initio potential it is necessary to evaluate the torsional contributions of the other force field terms and substract them from the QM profile [50, 51]. These contributions $U_C(\varphi_1)$ have been calculated from the logarithm of the nonbonded torsional angle distribution $P_C(\varphi_1)$ obtained from a separate MD simulation of an isolated T6 molecule at 600 K, in which the explicit FF torsional potential term $U_{FF}(\varphi_i)$ (fourth column in table 1) was fixed to zero. The difference between the QM and the nonbonded torsional potential $U_{FF}(\varphi_1) = U_{VTZ}(\varphi_1) + k_B T \ln P_C(\varphi_1)$ has then been fitted with a truncated Fourier series expansion that has been used as the new effective FF torsional potential, whose parameters are reported in table 1.

For a first validation of the force field we verified, like in reference [48], its capability of reproducing the crystalline cells of the two different monoclinic polymorphs of T6. We built the different crystallographic cells with the specific tool in Mercury 1.4.2 software [52], and through the replica of a single cell in three dimensions we obtained two small T6 crystals, used as starting configuration for Molecular Dynamics simulations. The simulated LT T6 crystal is a 3×6×3 replica of the single cell (108 molecules), while the HT T6 cell is replicated 1×5×7 on each single cell dimension (140 molecules). The LT and HT initial samples used in the MD simulation were equilibrated with the NAMD [53] software with simulation time 10 ns and temperature set to 292 K and 295 K respectively. As shown in table 2, the properties of the simulated cells are comparable with the experimental ones, and despite the relative simplicity of our potential energy function, the force field demonstrates performances comparable to the ones specifically obtained by Marcon et al. [48] and Della Valle et al. [54] for these crystalline phases.

3.1 Liquid crystal phases

Our first aim is to investigate if anisotropic phases exist between the crystalline and the isotropic one and to classify them. To this end we started heating progressively a LT sample composed of 140 molecules at T > 570 K up to 700 K with a typical production time of 60 ns and a time step of 1 fs. Every sample was equilibrated by simulations in NPT condition (P=1 atm) using periodic boundary conditions (PBC), Berendsen thermostat and anisotropic Berendsen barostat [55]. Electrostatic contributions were evaluated with the Particle Mesh Ewald method [56] using 1.2 for each box side and 3rd order splines; the scaling factors for 1–4 electrostatic Lennard Jones and intramolecular interactions were set to 5/6 and to 1/2 respectively [36]. It is important to remind here that the FF torsional parameters reported in table 1 are valid only for this choice of the 1–4 scaling factors.

For these N = 140 molecules samples we found a large ($\sim 20\%$) change in density at T $\sim$ 580K, possibly corresponding to a crystal to smectic transition. However we had difficulty in assessing the smectic character and even in locating the isotropisation temperature, due to the small sample size. For a more detailed investigation we thus prepared and employed larger samples of N = 1120 T6 molecules (49280 atoms) by replicating the small samples at each temperature twice along each dimension and re-equilibrating these for 5 ns; we then performed production runs for further 20 ns. In addition we heated the larger sample at 650 K to even higher temperatures to locate the nematic-isotropic transition temperature, reaching a total production time of $\sim$ 20 ns. For all these runs we have characterized the phases obtained in terms of density, order parameter, radial distribution function, energy and translational diffusion coefficient, and studied their variations with temperature. Starting with the density as a function of temperature in fig. 3 we see evidences of several phase transitions: a first large jump of about 0.2 g/cm^3 between 575 K and 580 K, and at higher temperatures an almost monotonical decrease with two small humps around T = 605 K and 665 K. To characterize the nature of the phases we proceeded to examine the orientational order parameter $\langle P_2 \rangle$, that measures the average degree of alignment of a molecular axis $\mathbf{u}$ along the preferred direction $\mathbf{n}$ (the director):

$$\langle P_2 \rangle = \left\langle \frac{3}{2}(\mathbf{u} \cdot \mathbf{n})^2 - \frac{1}{2} \right\rangle \tag{1}$$

to give an instantaneous $P_2(t)$ and a time average of this. The choice of the reference molecular direction $\mathbf{u}$ is not unique and here we have chosen for the prolate molecule T6 the eigenvector of the instantaneous T6 inertia tensor corresponding to the lowest eigenvalue. Following a well-established procedure in LC simulations [57] the scalar order parameter P_2 at time t can be determined for each configuration by setting up and diagonalizing the ordering matrix, $\mathbf{Q}$:

$$\mathbf{Q}(t) = \sum_{i=1}^{N}[3\mathbf{u}_i(t) \otimes \mathbf{u}_i(t) - \mathbf{I}]/(2N) \tag{2}$$

where $\mathbf{u}_i(t)$ is the axis of molecule i, $\mathbf{I}$ is the identity matrix and the sum runs over all the N molecules of the sample. The instantaneous order parameter $P_2(t)$ corresponds to the largest eigenvalue of $\mathbf{Q}(t)$, while the related eigenvector is the instantaneous director $\mathbf{n}(t)$. Examining the ensemble-averaged orientational order parameter $\langle P_2 \rangle$, (fig. 4) we see two small but appreciable jumps approximately located at 577.5 K and 607.5 K and a more significant and well defined drop between 665 K and 670 K, where the order parameter reaches effectively isotropic values ($\langle P_2 \rangle < 0.2$) and the clearing transition occurs. It is also interesting to note the system-size effects which determine, except for the first phase transition at the 577.5 K, that these transitions are less pronounced and appear at a temperature of about 15 K higher for the small sample than in the larger one.

From the analysis of the density and order parameter temperature trends, three different phase transitions then appear: the one at lower temperature corresponds to the melting of the crystal into a less dense and ordered phase; this phase eventually changes to a slightly less ordered one at about 607.5 K and finally at 665 K (clearing temperature) an isotropic phase appears. To better characterize the nature of the phases obtained, especially the ones intermediate between the crystal and the isotropic one, a knowlegde of the positional order and structure can be helpful and we have acccessed it as customary through the calculation of the radial distribution function (rdf):

$$g(r) = \frac{V}{4\pi r^2 N}\langle\delta(r - r_{ij})\rangle_{ij} \tag{3}$$

where r_{ij} is the distance between T6 centers of mass of molecules i and j, N is the total number of molecules, V is the volume. From the rdf plots (fig. 5) we note, as expected, a very structured distribution corresponding to the crystal phase at 575 K,

phase we observe the presence of various peaks indicating significant positional order at long range and suggesting the presence of layers, typical of a smectic phase. Increasing the temperature we see instead at 625 K and 675 K that the rdf is more liquid-like and only one or two short range peaks representing correlated shells of molecules are visible: considering that at 625 K we have also orientational order (fig. 4) is then possible to classify the corresponding phase as a nematic one; we verified that in all ordered phases the short range peak at about 5 Å corresponds to first neighboring molecules in herringbone configuration, with the molecular planes not lying parallel but making an angle of about 60 degrees. The phase that appears at the highest temperature is instead devoid of orientational and positional order - only the first peak of the rdf survives - consistently with an isotropic liquid phase.

Simulations allow to compute enthalpies as function of temperature via the textbook equation $\langle H(T) \rangle = \langle U(T) \rangle + p \langle V(T) \rangle$, where $\langle U(T) \rangle$ and $\langle V(T) \rangle$ are the average value of the force field energy and of the box volume at a given temperature and p is the external pressure. From the calculated values of enthalpy we estimated the transition enthalpies (ΔH_{trs}) and entropies (ΔS_{trs}), reported in table 3. We notice that the transition entropy value is significant for the crystal–smectic transition corresponding to a strong first order character, while for the other two transitions it is within our the experimental uncertainty. These values have been compared with the experimental data presents in literature for substituted liquid crystalline oligothiophenes [58, 59], finding a qualitative agreement with experiment for these different but related compounds. Moreover, the available experimental data for T6 crystal-mesophase transition enthalpy [11], $10 - 11$ kcal/mol measured with DSC, is in good agreement with our simulated value of 12.1 kcal/mol.

3.2 Characterization of the smectic phase

The presence of the layered molecular organization typical of smectics is confirmed by the typical sinusoidal trend of the density distribution function $\rho(z)$, where z is the projection of the intermolecular vector along the normal to the layers. The scaled $\rho(z)$ can be expanded in a Fourier series [60–62]:

$$\rho(z) = \rho_0 \left[1 + \langle \tau_1 \rangle \cos \left(q_S z \right) + \ldots + \langle \tau_n \rangle \cos \left(n q_S z \right) \right] \tag{4}$$

parameters, $q_S = \frac{2\pi}{d}$ is the wavevector of the density wave, d the interlayer distance. From figure 6 we can notice that indeed the linear density $\rho(z)$ from T=580 K to T=605 K follows the oscillatory behaviour predicted by equation 4, characteristic of a smectic A phase [62]. To obtain an estimate of the first non–vanishing smectic parameter $\langle\tau_1\rangle$ and of the layer spacing d we fitted the $\rho(z)$ shown in figure 6 with equation 4 truncated at the first two terms, obtaining the values reported in table 4. The low root mean square errors of the fit indicate that the first order approximation is very good for this specific system and that the fit parameters are physically meaningful. The layer spacing appears to be constant with temperature, as indicated also by the positions of the peaks of $\rho(z)$ in figure 6, and its value of 26.2 Å is comparable with the SS-trans molecular length of 26.5 Å. The good agreement between the periodicity of $\rho(z)$ and the molecular size indicates a negligible intergiditation between the layers. Finally the smectic order parameter $\langle\tau_1\rangle$ decreases gradually with temperature, confirming a second order or very weak first order transition from the smectic to the nematic phase already indicated by the low transition enthalpy in table 3). A further confirmation of the fluidity and of the anisotropic nature of the high temperature phases obtained can be verified by the translational diffusion tensor components:

$$D_{ii} = \lim_{t\to\infty} \frac{\langle (r_i(0) - r_i(t))^2\rangle}{2t} \tag{5}$$

where r_i is the component along the axis i=x,y,z of the director frame (the eigenvectors of $\mathbf{Q}$, eq. 2) of the molecular center of mass position vector for each molecule. The limit for $t \to \infty$ in equation 5 has been in practice approximated with the value for t=5 ns, and the diffusion coefficients parallel and perpendicular to the director shown in figure 7, correspond respectively to D_{zz} and $(D_{xx} + D_{yy})/2$, while D_{iso} is calculated as $(D_{xx} + D_{yy} + D_{zz})/3$.

As expected for a solid phase, the diffusion coefficient is negligible below the melting temperature, and increases with small but clearly visible jumps at the cry–sm, sm–nem and nem–iso transitions. In particular it exhibits a faster diffusion in the direction parallel to the phase director, not only in the nematic but also in the smectic phase. This dealing, somehow unexpected within the folklore of a smectic as a collection of independent two dimensional layers, but instead typical of the nematic phase, has been nevertheless reported in other smectic phases, such as the double

produced by suspensions of rod-like viruses [64]. Such a behaviour has been related to the extent of positional order and the rigidity of the smectic layers and maybe more interestingly, to the order of the smectic-nematic phase transition which is generally present at higher temperature [65,66]: if this transition is weak (like here), the smectic is believed to exhibit a "nematic-like" diffusional behavior, as it seems the case for T6.

To verify that the positional order is not a legacy of the original crystal starting configuration and more generally the thermodynamic stability of the smectic phase, we have attempted also to prepare a smectic sample by cooling from a nematic state point. We thus started from a previously equilibrated configuration at 610 K and we cooled instantaneously at the temperature of 600 K, hence below the smectic-nematic transition temperature obtained by heating runs. After 20 ns, smectic order was achieved, demonstrating that the smectic–nematic transition is reversible and not monotropic and confirming the satisfactory equilibration of previous heating runs. In fact the obtained mesophase shows $\rho(z)$, orientational order parameter, density and diffusion coefficients very similar to the ones obtained in the heating run (table 5).

3.3   Molecular Shape

The molecular shape is an important parameter in understanding LC phase stability and the change in transition temperatures induced by small chemical modifications [28, 31]. For instance we have shown by atomistic simulations that the odd-even effect in the transition temperature of the homologue series of cinnamate [28] and n-alkyl cyanobiphenyl series [31] is related to the effective average molecular length/breadth ratio: its increase leads to an enhancement of the ordered phase stability and thus of the nematic-isotropic transition temperature. The difficulty in using this concept as a predictive tool lies in the need of employing the actual shape of the molecule and in the fact that this will be determined by several possible conformations, differently populated as temperature changes. In T6 the effect is particularly interesting given the relatively weak inter-ring torsional barrier (fig. 2) and that an occasional syn–anti conversion around one of the bonds connecting two thiophene moieties can lead to a significant geometrical change, and affect the relaxation energies of the neutral and charged molecules which are so relevant for the

note that the probability of finding thiophene molecules with a central dihedral angle values different from 180° (linear planar shape) increases with temperature, and that at high T almost all torsional angles become populated.

For purely geometrical reasons, given that the thiophene-thiophene bonds are not parallel to the long molecular axis, the torsional disorder is expected to reduce the molecular dimensions. To quantify them we consider the sides r_l ($l = x, y, z$) of the minimal rectangular box containing the molecule rotated in its inertial frame as molecular size indicators, so the average molecular length is defined as $\langle r_z \rangle$ and molecular breadth as $\langle (r_x + r_y)/2 \rangle$ [28,31]. The average molecular length (fig. 9 left), having a value of ~ 27 Å in the crystal, suddenly lowers to ~ 26.6 Å at the smectic transition, and thereafter continues to decrease with a marked temperature dependence, clearly related to the average value of the cosine of central thiophene–thiophene dihedral (inset of fig. 8). The distribution of the aspect ratio (length/breadth, fig. 9, right) reflects this behaviour, highlighting the conformational change from a linear to a bent shape. In fact the most probable conformation (peak of the distribution) shifts towards lower values, and the distribution itself gets wider with increasing temperature. In the crystal phase the aspect ratio is ~ 4.5; increasing the temperature a contraction of the effective size anisotropy and a broadening of the distribution is observed.

The conformational disorder has as further consequence the breaking of the molecular symmetry and the increase of the molecular dipole: this effect, which here is induced by the temperature increase only, has also been attributed to be the driving force for T6 adsorption energy on clean gold surfaces [68]. In fig 10 we report the average value of dipole moment of T6 molecule as function of the simulated temperatures and we note that this quantity nearly doubles at the crystal-smectic transition. The prevalent component is the one perpendicular to the long molecular axis ($|\mu|_\perp$, about 1 Debye in the high temperature phases), suggesting a negative dielectric anisotropy and susceptivity both in the smectic and in the nematic phases, and the possibility of aligning T6 liquid crystalline phases with external electric fields.

Given that T6 would be inevitably employed in potential organic electronic applications at room temperature, the bent conformations just discussed seem difficult to reconcile with the flat conformations that would be optimal for high mobility. We have thus simulated T6 cooling and examined if the bent structures can be trapped by glass formation and to test this the hard way we have chosen a very fast cooling that should enhance the conformational trapping. We have cooled from the high temperature LC phases of T6 directly to room temperature (298 K) using as starting configurations the equilibrated samples respectively in nematic (from T6 simulated at 650 K) and in the smectic phase (from T6 at 590 K); the samples have been equilibrated for 40 ns and the observables have been calculated during a further 10 ns run. Both samples reached well ordered configurations with very similar properties (see tab. 5), even if less packed and more disordered than the original crystal structure, as it can be noticed by comparing the radial distribution functions in figure 11, and from the lower value of density (1.44 of the "glassy" samples vs 1.53 g/cm^3 for the crystal). Nevertheless the snapshots (figure 11) reveal a substantial rearrangement of the molecules in a crystal-like packing, suggesting that with more realistic (i.e. slower) cooling rates well formed crystals could be obtained starting from T6 LC phases; the fact that the conformational disorder obtained is very low $\langle \cos \varphi_1 \rangle = 0.94 - 0.95$ and comparable to the one of the crystal strengthens this hypothesis.

4   Conclusions

The high temperature phase behaviour of sexithiophene was studied with atomistic Molecular Dynamics simulations, by performing progressive heating a crystalline sample of 1120 molecules of the "low temperature" polymorph. We detected a phase transition from crystal to liquid crystal at about 580 K, in agreement with experiment [2, 10, 11]; the latter phase shows positional order and can be classified as a smectic. The transition is associated to a relevant density variation (from 1.4 to 1.2 g/cm^3) and to strong conformational changes of T6, namely the molecule in the liquid crystal phase easily assumes a bent shape, deviating from the planar structure typical of the crystal phase. The reversibility of the smectic–nematic transition was assessed as we obtained smectic ordering also by cooling a nematic sample. At 610 K

values for the order parameters, diffusion coefficients and the average molecular dipole of T6 - connected to molecular deformations - as a function of temperature and we hope these findings will stimulate future experimental determinations.

5   Acknowledgements

References

[1] D. Fichou. Structural order in conjugated oligothiophenes and its implications on opto-electronic devices. *J. Mater. Chem.*, 10:571, 2000.

[2] H. E. Katz, L. Torsi, and A. Dodabalapur. Synthesis, material properties, and transistor performance of highly pure thiophene oligomers. *Chem. Mater.*, 7:2235, 1995.

[3] G. Horowitz. Organic field-effect transistors. *Adv. Mater.*, 10:365, 1998.

[4] J. Sakai, T. Taima, T. Yamanari, and K. Saito. Annealing effect in the sexithiophene:c70 small molecule bulk heterojunction organic photovoltaic cells. *Sol. Energy Mat. Sol. Cells*, 93:1149, 2009.

[5] J. Cornil, J.-P. Calbert, D. Beljonne, R. Silbey, and J.-L. Brédas. Charge transport versus optical properties in semiconducting crystalline organic thin films. *Adv. Mater.*, 21:978–983, 2000.

[6] H. E. Katz and Z. N. Bao. The physical chemistry of organic field-effect transistors. *J. Phys. Chem. B*, 104:671, 1999.

[7] A. J. Lovinger, D. D. Davis, A. Dodabalapur, H. E. Katz, and L. Torsi. Single-crystal and polycrystalline morphology of the thiophene-based semiconductor α-hexathienyl (α-6t). *Macromolecules*, 29:4952, 1996.

D. Sparrowe, S. Tierney, R. Wagner, W. M. Zhang, M. L. Chabinyc, R. J. Kline, M. D. McGehee, and M. F. Toney. Liquid-crystalline semiconducting polymers with high charge-carrier mobility. *Nature Mater.*, 5:328, 2006.

[9] M. M. Ling and Z. N. Bao. Thin film deposition, patterning, and printing in organic thin film transistor. *Chem. Mater.*, 16:4824, 2004.

[10] C. Taliani, R. Zamboni, G. Ruani, S. Rossini, and R. Lazzaroni. New rigid rod liquid crystal molecule precursor of conjugated polymers: α-sexithienyl. *J. Mol. Electron.*, 6:225, 1990.

[11] S. Destri, M. Mascherpa, and W. Porzio. Mesophase formation in α-sexithienyl at high temperature - an x-ray diffraction study. *Adv. Mater.*, 5:43, 1993.

[12] G. Horowitz, M. E. Hajlaoui, and R. Hajlaoui. Temperature and gate voltage dependence of hole mobility in polycrystalline oligothiophene thin film transistors. *J. Appl. Phys.*, 87:4456, 2000.

[13] F. Dinelli, M. Murgia, P. Levy, M. Cavallini, F. Biscarini, and D. M. de Leeuw. Spatially correlated charge transport in organic thin film transistors. *Phys. Rev. Lett.*, 92:116802, 2004.

[14] C. D. Dimitrakopoulos and D. J. Mascaro. Organic thin-film transistors: A review of recent advances. *IBM J. Res. Dev.*, 45:11, 2001.

[15] M. E. Rose. *Handbook of Oligo- and Polythiophenes*. Academic, New York, 1998.

[16] F. Biscarini, P. Samorì, A. Lauria, P. Ostoja, R. Zamboni, C. Taliani, P. Viville, R. Lazzaroni, and J. L. Brédas. Morphology and roughness of high-vacuum sublimed oligomer thin films. *Thin Solid Films*, 284-285:439, 1996.

[17] M. Kramer and V. Hoffman. Infrared spectroscopic characterization of orientation and order of thin oligothiophene films. *Opt. Mater.*, 9:65, 1998.

[18] F. Biscarini, R. Zamboni, P. Samorì, P. Ostoja, and C. Taliani. Growth of conjugated oligomer thin films studied by atomic-force microscopy. *Phys. Rev. B*, 52:14868, 1995.

 termination of the crystal structure and orientation of vacuum evaporated sexithiophene films. *Adv. Mater.*, 5:461, 1993.

[20] N. S. Sariciftci, U. Lemmer, D. Vacar, A. J. Heeger, and R. A. I. Janssen. Polarized photoluminescence of oligothiophenes in nematic liquid crystalline matrices. *Adv. Mater.*, 8:651, 1996.

[21] L. C. Terbeek, D. S. Zimmerman, and E. E. Burnell. The conformation of $2, 2'$-dithiophene in nematic solvents determined by $^1H - NMR$. *Mol. Phys.*, 74:1027, 1991.

[22] G. Horowitz, B. Bachet, A. Yassar, P. Lang, F. Demanze, J. L. Fave and F. Garnier. Growth and characterization of sexithiophene single crystals. *Chem. Mater.*, 7:1337, 1995.

[23] T. Siegrist, R. M. Fleming, R. C. Haddon, R. A. Laudise, A. J. Lovinger, H. E. Katz, P. Bridenbaugh, and D. D. Davis. The crystal structure of the high-temperature polymorph of α-hexathienyl (α-6t/ht). *J. Mol. Res.*, 10, 1995.

[24] Cambridge Crystallographic Data Centre. http://www.ccdc.cam.ac.uk/.

[25] N. A. Zafiropoulos, E-J. Choi, T. J. Dingemans, W. Lin, and E. T. Samulski. New all-aromatic liquid crystal architectures. *Chem. Mater.*, 20:3821–3831, 2008.

[26] S. Kuiper, W. F. Jager, T. J. Dingemans, and S. J. Picken. Liquid crystalline properties of all symmetric p-phenylene and 2,5-thiophene pentamers. *Liq. Cryst.*, 36:389–396, 2009.

[27] M.-H. Yoon, A. Facchetti, C. E. Stern, and T. J. Marks. Fluorocarbon-modified organic semiconductors: Molecular architecture, electronic, and crystal structure tuning of arene- versus fluoroarene-thiophene oligomer thin-film. *J. Am. Chem. Soc.*, 128:5792–5801, 2006.

[28] R. Berardi, L. Muccioli, and C. Zannoni. Can nematic transitions be predicted by atomistic simulations? a computational study of the odd-even effect. *ChemPhysChem*, 5:104, 2004.

in the isotropic phase of a liquid crystal. *J. Phys. Chem. B*, 111:1475, 2007.

[30] M. Cifelli, L. De Gaetani, G. Prampolini, and A. Tani. Atomistic computer simulation and experimental study on the dynamics of the n-cyanobiphenyls mesogenic series. *J. Phys. Chem. B*, 112:9777, 2008.

[31] G. Tiberio, L. Muccioli, R. Berardi, and C. Zannoni. Towards in silico liquid crystals. predicting molecular organization and phase transitions for n-cyanobiphenyls via molecular dynamics simulations. *ChemPhysChem*, 10:125, 2009.

[32] L. De Gaetani and G. Prampolini. Computational study through atomistic potentials of a partial bilayer liquid crystal: structure and dynamics. *Soft Matter*, 5:3517–3526, 2009.

[33] M. R. Wilson. Progress in computer simulations of liquid crystals. *Int. Rev. Phys. Chem.*, 24:421–455, 2005.

[34] S. J. Weiner, P. A. Kollman, D. A. Case, U. C. Singh, C. Ghio, G. Alagona, S. Profeta, and P. Weiner. A new force field for molecular mechanical simulation of nucleic acids and proteins. *J. Am. Chem. Soc.*, 106:765, 1984.

[35] S. J. Weiner, P. A. Kollman, D. T. Nguyen, and D. A. Case. An all atom force field for simulations of proteins and nucleic acids. *J. Comput. Chem.*, 7:230, 1986.

[36] W. D. Cornell, P. Cieplak, C. I. Bayly, I. R. Gould, K. M. Merz, D. M. Ferguson, D. C. Spellmeyer, T. Fox, J. W. Caldwell, and P. A. Kollman. A second generation force field for the simulation of proteins and nucleic acids. *J. Am. Chem. Soc.*, 117:5179, 1995.

[37] J. Wang, R. M. Wolf, J. W. Caldwell, P. A. Kollman, and D. A. Case. Development and testing of a general amber force field. *J. Comput. Chem.*, 25:1157, 2004.

[38] B. H. Besler, K. M. Merz Jr., and P. A. Kollman. Atomic charges derived from semiempirical methods. *J. Comput. Chem.*, 11:431, 1990.

[40] J. L. Brédas, G. B. Street, B. Thèmans, and J. M. André. Organic polymers based on aromatic rings (polyparaphenylene, polypyrrole, polythiophene): Evolution of the electronic properties as a function of the torsion angle between adjacent rings. *J. Chem. Phys.*, 83:1323, 1985.

[41] O. A. Gus'kova, P. G. Khalatur, and A. R. Khokhlov. Self-assembled polythiophene-based nanostructures: Numerical studies. *Macromol. Theory Simul.*, 18:219, 2009 and references therein.

[42] F. Rodriguez-Ropero, J. Casanovas, and C. Aleman. Solvation of 2,2′-bithiophene: Influence of the first solvation shell in the properties of pi-conjugated systems. *Chem. Phys. Lett.*, 416:331, 2005.

[43] D. R. Ferro, W. Porzio, S. Destri, M. Ragazzi, and S. Bruckner. Application of molecular mechanics to refine and understand the crystal structure of polythiophene and its oligomers. *Macromol. Theory Simul.*, 6:713, 1997.

[44] R. Berardi, F. Spinozzi, and C. Zannoni. The rotational-conformational distribution of $2, 2'$-bithienyl in liquid crystals. *Liq. Cryst.*, 16:381, 1994.

[45] C. Alemán, V. M. Domingo, L. Fajarí, L. Juliá, and A. Karpfen. Molecular and electronic structures of heteroaromatic oligomers: Model compounds of polymers with quantum-well structures. *J. Org. Chem.*, 63:1041, 1998.

[46] G. Raos, A. Famulari, and V. Marcon. Computational reinvestigation of the bithiophene torsion potential. *Chem. Phys. Lett.*, 379:364, 2003.

[47] J. C. Sancho-Garcia and J. Cornil. Assessment of recently developed exchange-correlation functionals for the description of torsion potentials in -conjugated molecules. *J. Chem. Phys.*, 121:3096–3101, 2004.

[48] V. Marcon and G. Raos. Molecular modeling of crystalline oligothiophenes: testing and development of improved force fields. *J. Phys. Chem. B*, 108:18053, 2004.

[49] S. E. Koh, C. Risko, D. A. da Silva Filho, O. Kwon, A. Facchetti, J.-L. Brédas, T. J. Marks, and M. A. Ratner. Modeling electron and hole transport in

17

tronic structure properties. *Adv. Funct. Mater.*, 18:332–340, 2008.

[50] R. Berardi, G. Cainelli, P. Galletti, D. Giacomini, A. Gualandi, L. Muccioli, and C. Zannoni. Can the *pi*-facial selectivity of solvation be predicted by atomistic simulation? *J. Am. Chem. Soc.*, 127:10699–10706, 2005.

[51] G. Tiberio, L. Muccioli, R. Berardi, and C. Zannoni. How does the *trans-cis* photoisomerization of azobenzene take place in organic solvents? *Chem. Phys. Chem.*, in press, 2010.

[52] I. J. Bruno, J. C. Cole, P. R. Edgington, M. K . Kessler, C. F. Macrae, P. McGabe, J. Pearson, and R. Taylor. New software for searching the cambridge structural database and visualising crystal structures. *Acta Cryst.*, B58:389, 2002.

[53] J. C. Phillips, R. Braun, W. Wang, J. Gumbart, E. Tajkhorshid, E. Villa, C. Chipot, R. D. Skeel, L. Kale, and K. Schulten. Scalable molecular dynamics with NAMD. *J. Comput. Chem.*, 26:1781, 2005.

[54] A. Brillante, I. Bilotti, F. Biscarini, R. G. Della Valle, and E. Venuti. Polymorphs of α-sexithiophene probed by lattice phonon raman microscopy. *Chem. Phys.*, 328:125, 2006.

[55] H. J. C. Berendsen, J. P. M. Postma, A. Di Nola, and J. R. Haak. Molecular dynamics with coupling to an external bath. *J. Chem. Phys.*, 81:3684, 1984.

[56] U. Essmann, L. Perera, M. L. Berkowitz, T. A. Darden, H. Lee, and L. G. Pedersen. A smooth particle mesh Ewald method. *J. Chem. Phys.*, 101:8577–8593, 1995.

[57] C. Zannoni. Order parameters and orientational distributions in liquid crystals. In G. R. Luckhurst and G. W. Gray, editors, *The Molecular Physics of Liquid Crystals*, chapter 3, pages 51–83. Academic Press, London, 1979.

[58] M. Melucci, F. Favaretto, M. Gazzano, N. Camaioni, P. Maccamagni, P. Ostoja, M. Monari, and G. Barbarella. Liquid-crystalline rigid-core semiconductor oligothiophenes: Influence of molecular structure on phase behaviour and thin-film properties. *Chem. Eur. J.*, 13:10046, 2007.

18

metrical liquid crystalline oligothiophenes. Convenient synthesis and transition temperature engineering. *Eur. J. Org. Chem.*, page 1256, 2007.

[60] W. L. McMillan. X-ray scattering from liquid crystals. i. cholesteryl nonanoate and myristate. *Phys. Rev. A*, 6:936, 1972.

[61] P. G. de Gennes. *The Physics of Liquid Crystals*. Clarendon Press, Oxford, 1974.

[62] R. G. Marguta, E. Martín del Rio, and E de Miguel. Revisiting McMillan's theory of the smectic A phase. *J. Phys.: Condens. Matter*, 18:10335, 2006.

[63] S. V. Dvinskikh, I. Furó, H. Zimmermann, and A. Maliniak. Anisotropic self-diffusion in thermotropic liquid crystal by ^{1}H and ^{2}H pulse field gradient spin-echo NMR. *Phys. Rev. E*, 65:061701, 2002.

[64] M. P. Lettinga and E. Grelet. Self-diffusion of rodlike viruses through smectic layers. *Phys. Rev. Lett.*, 99:197802, 2007.

[65] O. Oishi and S. Miyajima. Inversion of self-diffusion anisotropy by chemical substitution in smectic a liquid crystals as evidenced by pgse experiment combined with a quadrupole-coil rotation. *J. Magn. Reson.*, 160:74–77, 2003.

[66] M. Cifelli and C. A. Veracini. Translational self diffusion anisotropy in the smectic a phase measured by a static fringe field gradient ^{1}H NMR diffusometry approach. *Phys. Chem. Chem. Phys.*, 7:34123415, 2005.

[67] D. A. da Silva Filho, V. Coropceanu, D. Fichou, N. E. Gruhn, T. G. Bill, J. Gierschner, J. Cornil, and J.-L. Brédas. Hole-vibronic coupling in oligothiophenes: impact of backbone torsional flexibility on relaxation energies. *Phil. Trans. R. Soc. A*, 365:1435–1452, 2007.

[68] N. Sändig, F. Biscarini, and F. Zerbetto. Driving force for the adsorption of sexithiophene on gold. *J. Phys. Chem. C*, 112:19516–19420, 2008.

Table 1: Fitting parameters for the T6 torsional potentials expressed as a Fourier series $U(\varphi_i) = \sum_{n=1}^{8} K_n \cos(n\varphi_i)$: central thiophene-thiophene dihedral calculated at B3LYP//cc-pVTZ level (φ_1 VTZ), end dihedral calculated at B3LYP//cc-pVDZ level (φ_3 VDZ), central dihedral as implemented in the molecular mechanics force field after the removal of the non-bonded contribution(φ_1 FF).

n	K_n [kcal/mol]		
	φ_1 VTZ	φ_3 VDZ	φ_1 FF
1	+0.295	+0.338	+0.465
2	-1.669	-1.340	-2.333
3	+0.090	+0.084	+0.131
4	+0.502	+0.487	+0.387
5	0.000	+0.020	-0.001
6	-0.026	-0.018	-0.048
7	+0.016	0.000	0.000
8	+0.030	0.000	0.000

Table 2: Simulation results for LT and HT polymorphs of T6. (a) Data from reference [22], (b) data from our simulation, (c) data from reference [54] (d) data from reference [48] and (e) data from reference [23].

T6	LT polymorph				HT polymorph		
	$\exp^a$	sim^b	sim^c	sim^d	$\exp^e$	sim^b	sim^c
ρ (g/cm^3)	1.553	1.509	1.579	1.515	1.55	1.52	1.61
a (Å)	44.708	45.650	45.001	45.509	9.1404	8.401	8.248
b (Å)	7.851	7.804	7.682	7.972	5.6843	5.983	5.798
c (Å)	6.029	6.113	6.023	5.974	20.672	21.527	21.499
α (deg)	90	89.70	90	90	90	90.23	90
β (deg)	90.76	89.52	89.97	88.43	97.78	93.86	95.81
γ (deg)	90	89.79	90	90	90	90.10	90
T (K)	292	292	292	298	295.65	295	295

Table 3: Values of transition temperature T_{trs} (in K), ΔH_{trs} (in kcal/mol) and ΔS_{trs} (in cal/(mol K)) for T6 transitions.

Transition			T_{trs}	ΔH_{trs}	ΔS_{trs}
iso	-	nem	667.5	0.4	-0.5
nem	-	sm	607.5	0.2	-0.3
sm	-	cry	577.5	12.1	-20.8

Table 4: Smectic order parameter τ_1 and interlayer distance d with relative standard deviation obtained by fitting the density distribution functions with the first two terms on the right hand side of Eq 4.

T (K)	τ_1	d (Å)	rms
580	0.82	26.2	0.06
585	0.79	26.2	0.05
590	0.63	26.2	0.03
595	0.51	26.2	0.02
600	0.21	26.2	0.00
605	0.03	26.4	0.00

Table 5: Density, order parameters and translational diffusion coefficients values confirm the reversibility of the smectic–nematic transition for a sample of 1120 T6 molecules at 600 K obtained from heating and cooling runs.

	ρ (g/cm^3)	$\langle P_2 \rangle$	$\langle \tau_1 \rangle$	d (Å)	$D_\perp$ (m^2/s)	$D_\parallel$ (m^2/s)
heating	1.15 ± 0.01	0.83 ± 0.02	0.21	26.3	9×10^{-10}	25×10^{-10}
cooling	1.15 ± 0.01	0.82 ± 0.02	0.18	26.2	9×10^{-10}	25×10^{-10}

Table 6: Density, order parameter and molecular shape properties from structures derived from the smectic–room transition (sm-amb) and the nem–room transition (nem-amb) with respect to the crystal phase.

T (K)	ρ (g/cm^3)	$\langle P_2 \rangle$	$\langle \cos \varphi_1 \rangle$	length (Å)	length/breath
298 (sm-amb)	1.44	0.97	0.95	26.99	4.50
298 (nem-amb)	1.44	0.97	0.94	27.03	4.58
292 (cry)	1.51	1.00	0.97	27.12	4.84
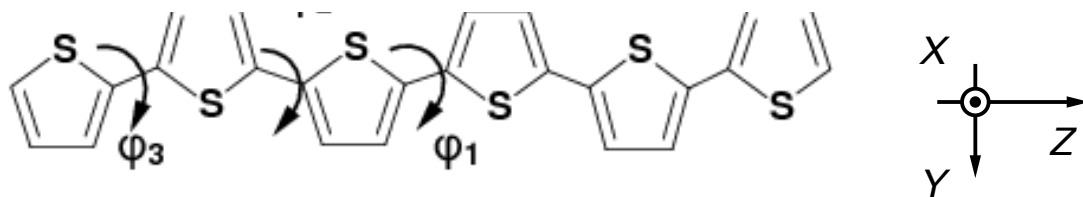
Figure 1: Chemical sketch of the α-sexithiophene molecule (T6), and of the molecular reference frame. The three different typologies of thiophene-thiophene torsion are indicated as φ_1, φ_2, φ_3.
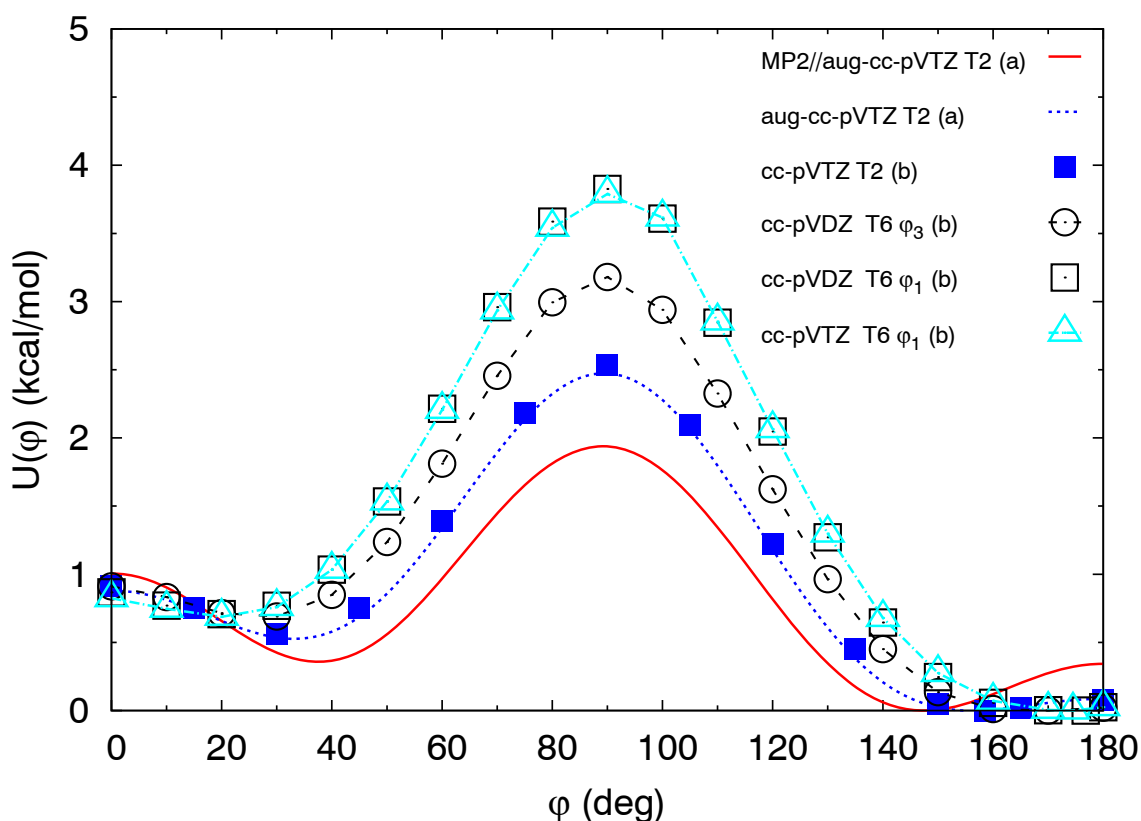
Figure 2: Torsional potential $U(\varphi)$ for thiophene-thiophene rotation for dithiophene and sexithiophene calculated at different levels: T2 MP2/aug-cc-pVTZ (red line) and B3LYP//aug-cc-pVTZ (blue dotted line) from reference [46]; T2 MP2/cc-pVTZ (blue squares); T6 terminal dihedral φ_3 with B3LYP//cc-pVDZ (black dotted line and empty circles) T6 central dihedral φ_1 with B3LYP//cc-pVDZ (black empty squares) and B3LYP//cc-pVTZ (empty cyan triangles).
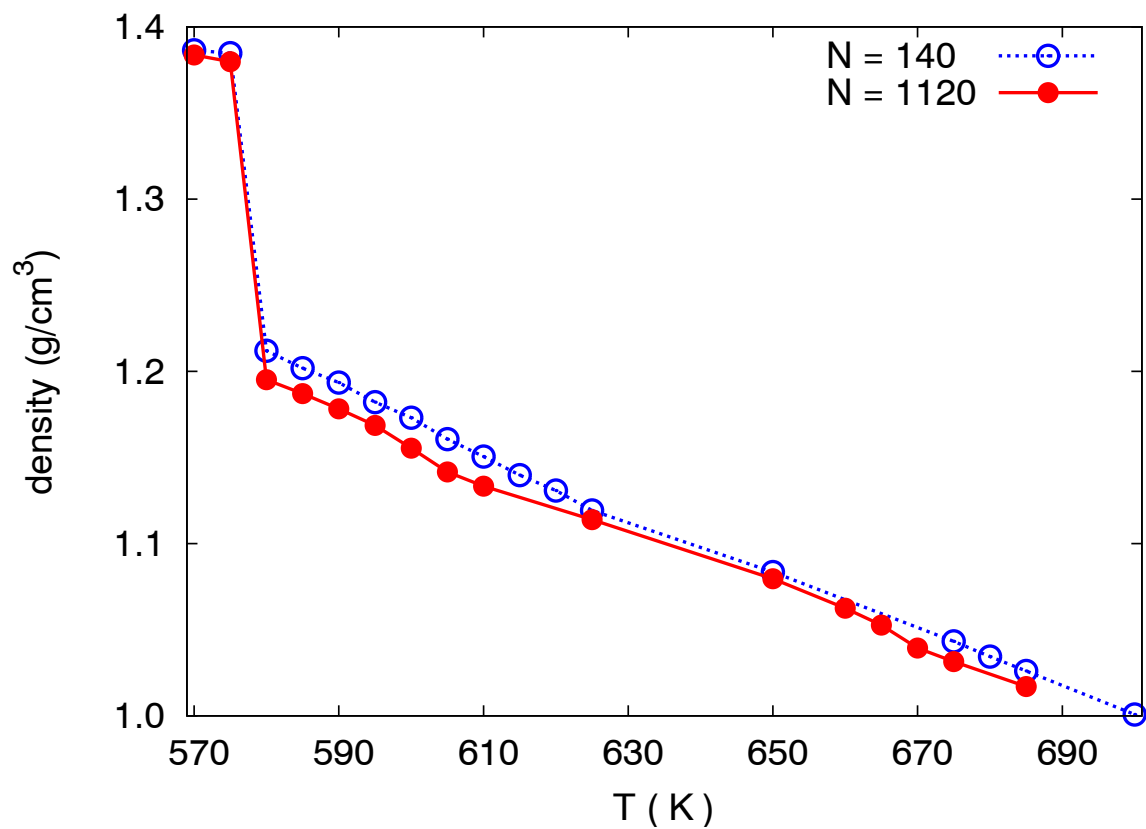
Figure 3: Density of N=140 and N=1120 T6 samples as function of temperature, showing that density is essentially unchanged by the increase in sample size.
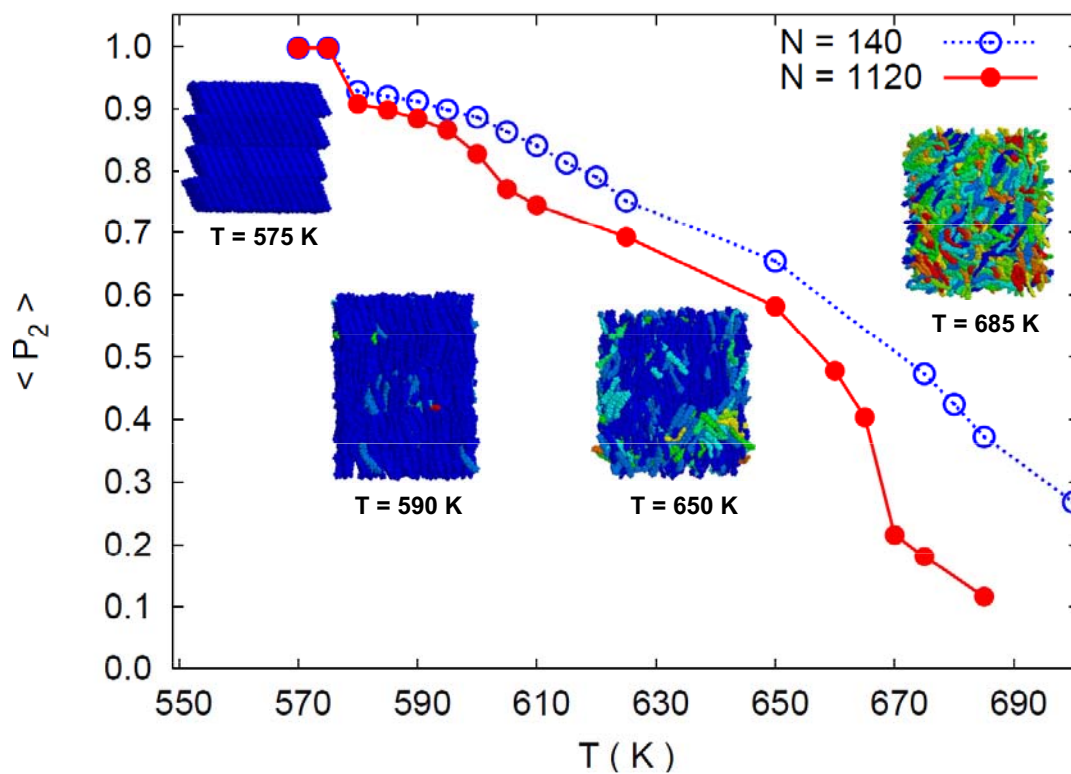
Figure 4: Orientational order parameter for the N=140 and N=1120 T6 samples as function of temperature, showing the importance of sufficiently large system size for locating the phase transitions. The snapshots of the different phases correspond, from the left to the right, to simulations at 575, 590, 650 and 685 K respectively. Molecules are color-coded according to the orientation of their reference axis **u** with the respect to the phase director **n**, ranging from from blue (parallel) to red (perpendicular)
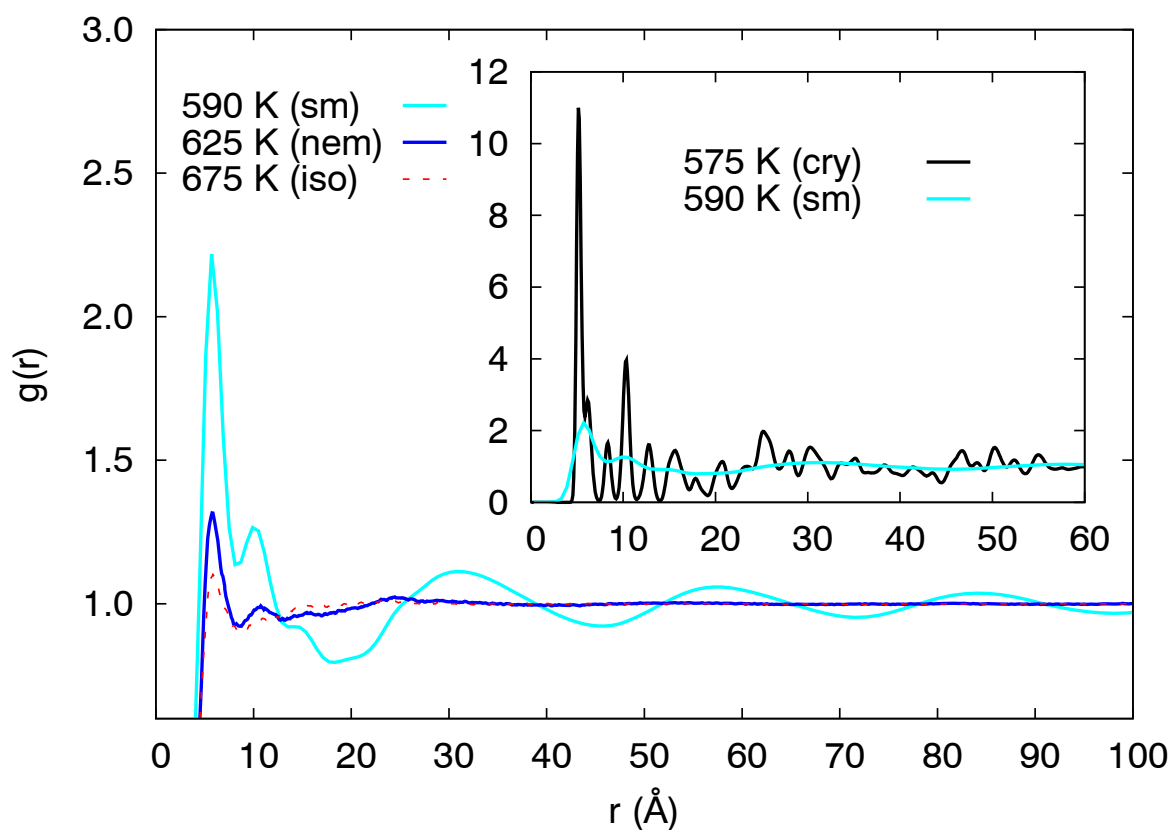
Figure 5: Comparison of the radial distribution function of T6 in the different phases: in the main plot, smectic (cyan) versus nematic (blue) and isotropic (red dashed line); in the inset, smectic (cyan) versus crystal phase (black).
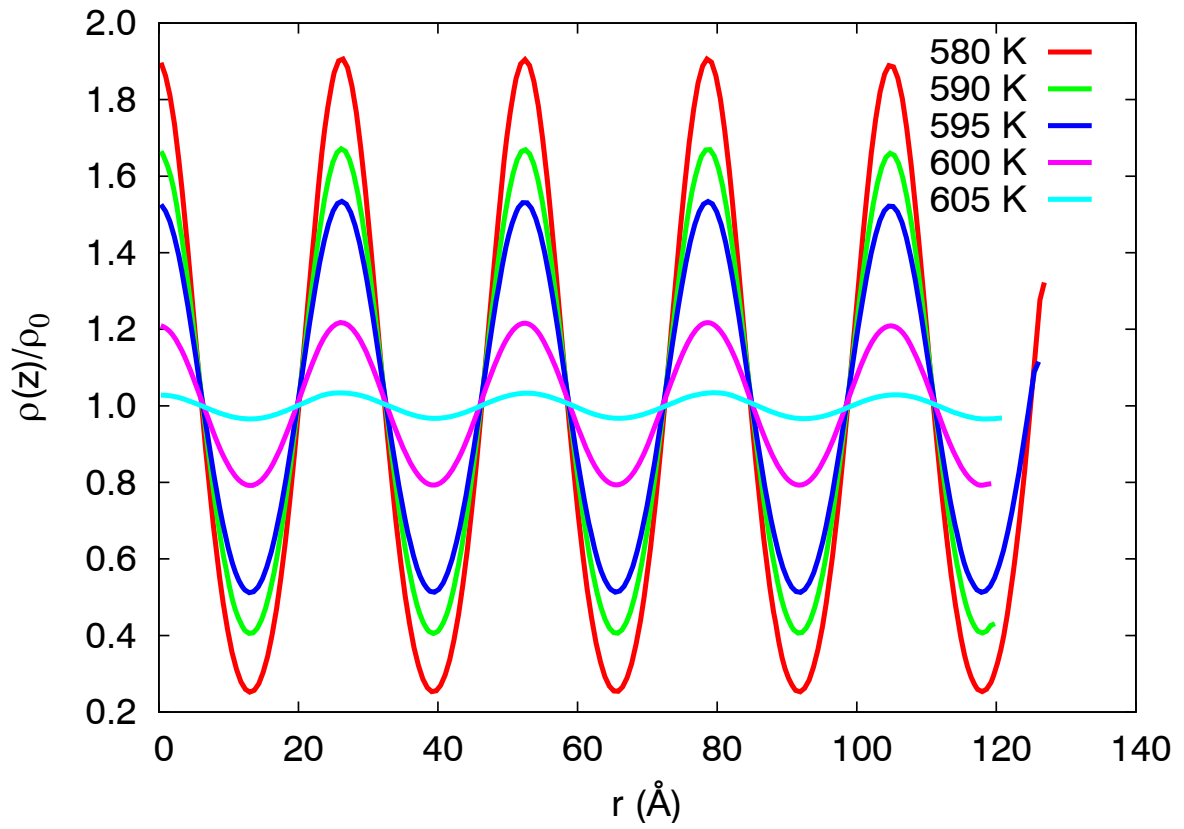
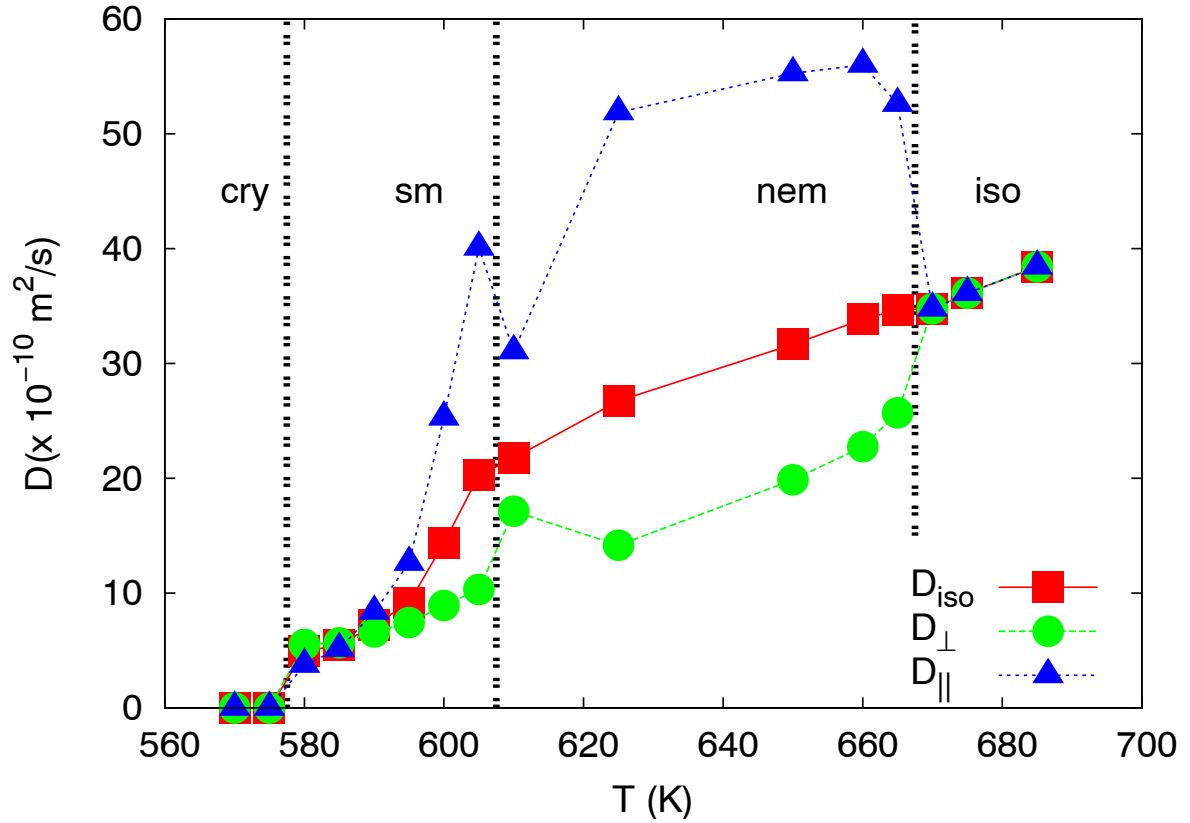Figure 6: Scaled density probability along the alignment direction z showing the existence of smectic layers.

Figure 7: Translational diffusion coefficients as functions of temperature for the N=1120 samples: isotropic ($D_{iso} = (D_{xx} + D_{yy} + D_{zz})/3$, red squares), perpendicular ($D_\perp = (D_{xx} + D_{yy})/2$, green circles) and parallel ($D_\parallel = D_{zz}$, blue triangles) to the phase director.
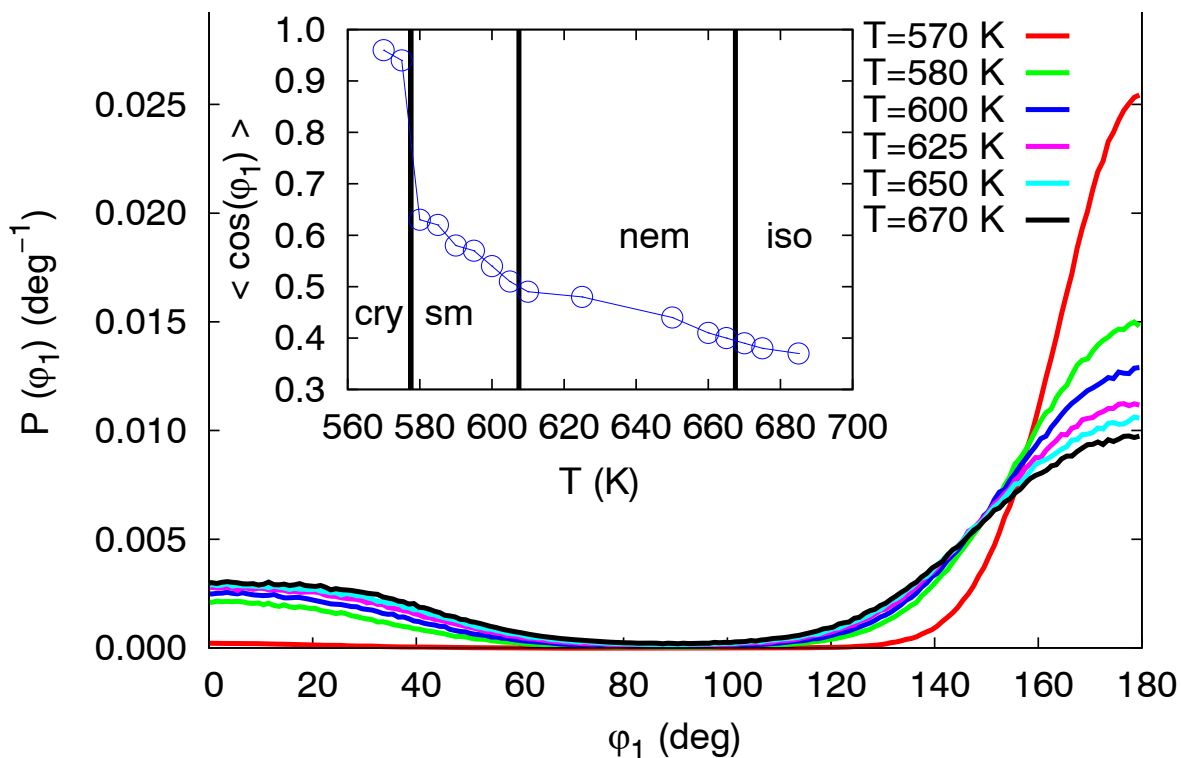
Figure 8: Distribution of the dihedral φ_1 between the central rings of the simulated phases. The average cosine of the angle versus temperature is plotted in the inset.
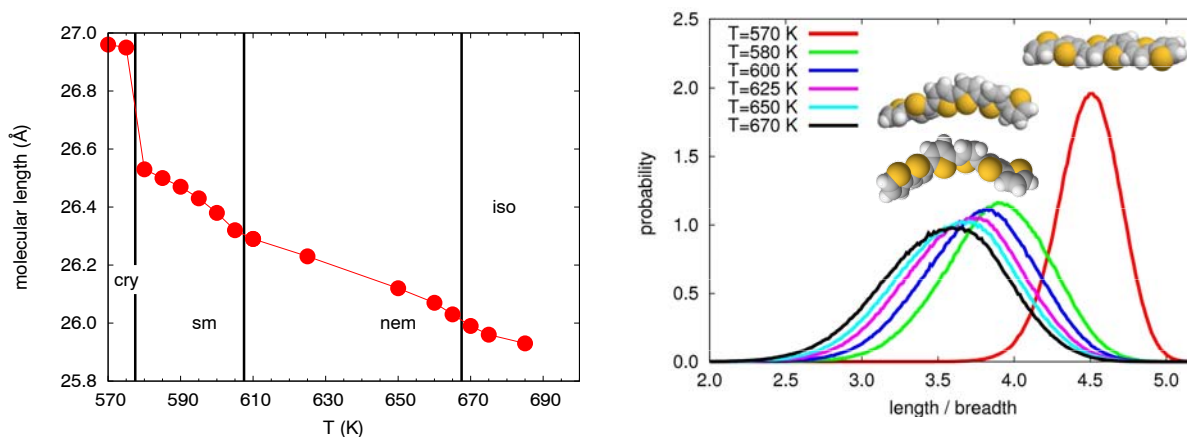

Figure 9: T6 average length of the simulated temperature (left) and distribution of molecular length to breadth ratio for the simulated phases (right). The space filling representation of three conformers extracted from the simulation is also shown.
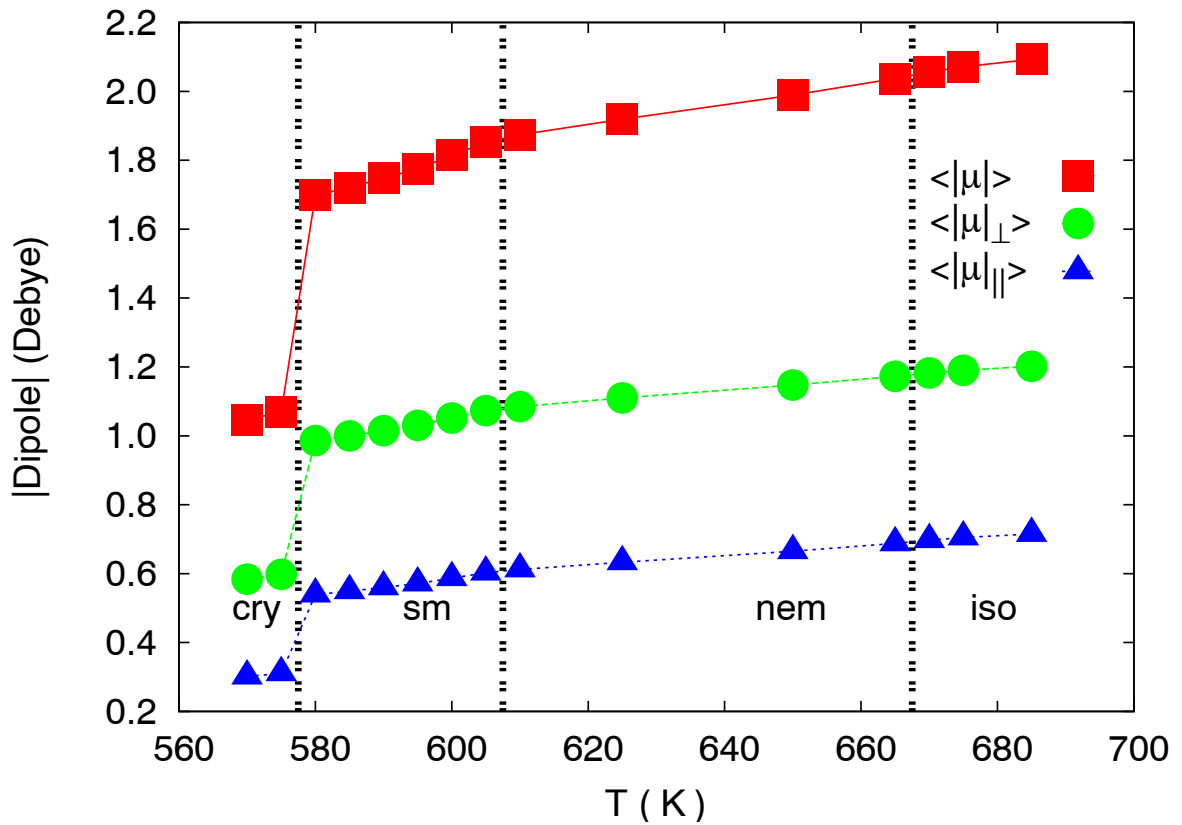
Figure 10: Average of the absolute value of total molecular dipole $|\mu|$ (red squares), and of its components perpendicular ($|\mu|_\perp$, green circles) and parallel ($|\mu|_\parallel$, blue triangles) to the long molecular axes, as function of temperature for the N=1120 samples.
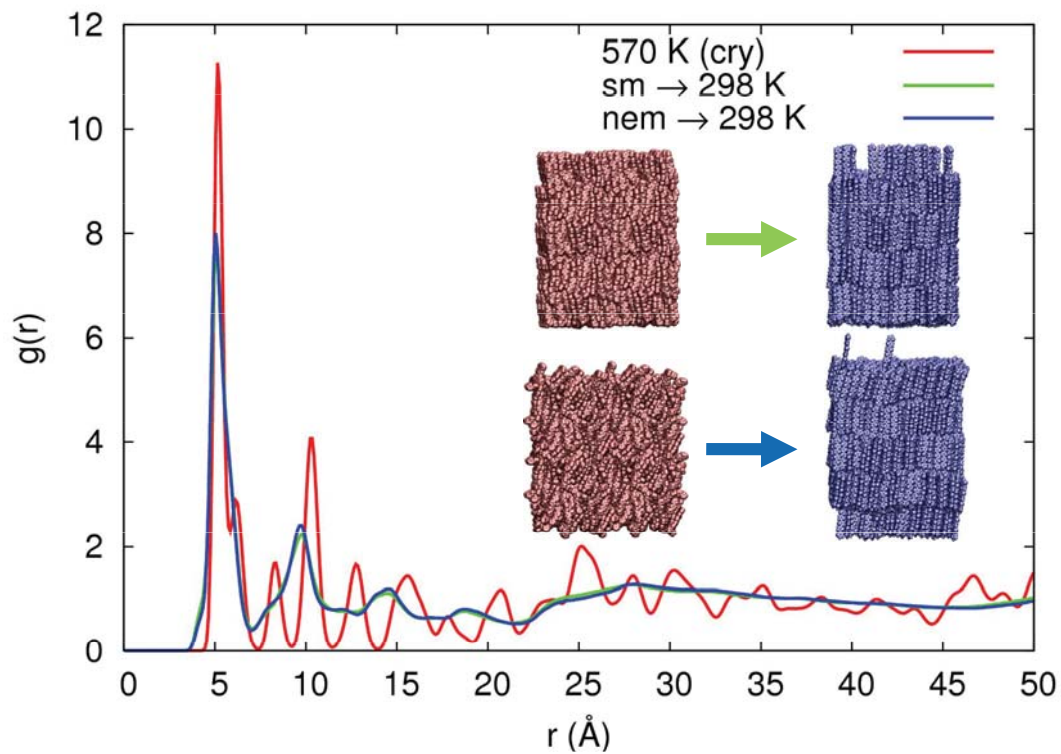
Figure 11: Radial distribution function of the cooled structures with respect to the crystal phase simulated at 570 K (red) and the smectic phase simulated at 580 K (black). The trends of the new morphologies (green and blue) are similar. The initial and final snapshots of cooling simulation at room temperature obtained from the nematic (top) and smectic phase (bottom) are shown as inset.